J. Fluid Mech. (2016), *vol.* 794, *pp.* 639–654. © Cambridge University Press 2016
doi:10.1017/jfm.2016.181

Effects of geometric confinement in quasi-2-D turbulent Rayleigh–Bénard convection

Shi-Di Huang[1] **and Ke-Qing Xia**[1,†]

[1]Department of Physics, The Chinese University of Hong Kong, Shatin, Hong Kong, China

(Received 9 November 2015; revised 26 January 2016; accepted 3 March 2016;
first published online 6 April 2016)

We report an experimental study of confinement effects in quasi-2-D turbulent Rayleigh–Bénard convection. The experiments were conducted in five rectangular cells with their height H and length L being the same and fixed, while the width W was different for each cell to produce lateral aspect ratios ($\Gamma = W/H$) of 0.6, 0.3, 0.2, 0.15 and 0.1. Direct flow field measurements reveal that the large-scale flow slows down as Γ decreases and there are more plumes travelling through the bulk region. Moreover, the reversal frequency of the large-scale flow is found to increase drastically in smaller Γ cells, by more than 1000-fold for the highest value of Rayleigh number reached in the experiment. The reversal frequency can be well described by a stochastic model developed by Ni *et al.* (*J. Fluid Mech.*, vol. 778, 2015, R5) and the probability density functions (PDF) of the time interval between successive reversals are found to follow Poisson statistics as in the 3-D system. It is further observed that the bulk temperature fluctuation increases significantly and its PDF changes from exponential to Gaussian as Γ decreases. The influences of geometric confinement on the global heat transport are also investigated. The measured Nu–Ra relationship suggests that, as the lateral aspect ratio decreases, the relative weight of the boundary layer contribution in the global heat transport increases compared to that from the bulk. These results demonstrate that in the quasi-2-D geometry, geometric confinement has strong effects on both the global and local properties in turbulent convective flows, which are very different from the previous findings in 3-D and true 2-D systems.

Key words: Bénard convection, plumes/thermals, turbulent flows

1. Introduction

Thermal turbulence is ubiquitous in both nature and industrial applications. Turbulent Rayleigh–Bénard (RB) convection, a fluid layer heated from the bottom and cooled from the top has become a paradigm for the study of general convection phenomena. Over the years, there have been extensive studies addressing how the heat transport and flow dynamics of turbulent RB convection are determined by two control parameters, i.e. the Rayleigh number $Ra = \alpha g \Delta T H^3/\nu\kappa$ and the Prandtl number $Pr = \nu/\kappa$, where ΔT is the temperature difference across the fluid layer of height H, g is the acceleration due to gravity and α, ν and κ are the thermal

† Email address for correspondence: kxia@phy.cuhk.edu.hk

expansion coefficient, the kinematic viscosity and the thermal diffusivity of the working fluid, respectively (for reviews, see Ahlers, Grossmann & Lohse 2009; Lohse & Xia 2010; Chillà & Schumacher 2012; Xia 2013). In laboratory experiments, the convective flows are always confined in containers with different geometries. It is generally believed that different geometric configurations will result in different flow structures and thus different associated flow properties. Therefore, the third control parameter that characterizes the effects of geometric confinement, aspect ratio Γ (lateral dimension of the fluid layer over its height), comes into the problem.

Most of the existing studies on the confinement effects in turbulent RB convection were made in 3-D geometry (Funfschilling *et al.* 2005; Nikolaenko *et al.* 2005; Sun *et al.* 2005*a*; Niemela & Sreenivasan 2006; du Puits, Resagk & Thess 2007; Xia, Sun & Cheung 2008; Bailon-Cuba, Emran & Schumacher 2010; Roche *et al.* 2010; Wu & Libchaber 2012; Zhou *et al.* 2012) and the general findings were: (i) the single-roll structure changes to a multi-roll pattern with increasing Γ; (ii) the heat transfer efficiency, characterized by the Nusselt number Nu, decreases slightly as Γ increases and the asymptotic large-Γ behaviour may have been reached for $\Gamma \gtrsim 10$. These findings have led one to conclude that the flow structures do not strongly influence the heat transport properties (Ahlers, Grossmann & Lohse 2009). Recently, there has been a growing interest in 2-D RB flow (Sugiyama *et al.* 2010; van der Poel, Stevens & Lohse 2011, 2013; van der Poel *et al.* 2012; Chandra & Verma 2013; Huang & Zhou 2013; Podvin & Sergent 2015). It was found that such a geometry will result in a stronger and more complicated Γ-dependence of Nu, which was ascribed to the different flow structures in the 2-D system (van der Poel *et al.* 2011, 2012, 2013). Although the flow dynamics in the 2-D system, which strictly can only be realized numerically, may share certain features with those in the quasi-2-D case (Sugiyama *et al.* 2010), a true 2-D system is fundamentally different from a quasi-2-D one. Indeed, recent studies by Huang *et al.* (2013) and Chong *et al.* (2015) found that simple geometric confinement in the quasi-2-D system can significantly enhance convective heat transport, which is brought about by the change in the dynamics and morphology of the thermal plumes. Such a striking phenomenon has not been observed in previous studies in 3-D and true 2-D systems. In this paper, we further investigate the confinement effects in quasi-2-D turbulent RB convection by experimentally studying various flow properties, including flow dynamics, local temperature fluctuation and global heat transport. The results will complement the findings reported in Huang *et al.* (2013) and Chong *et al.* (2015). As will be shown in the paper, in the quasi-2-D geometry, the geometric confinement not only can strongly influence the local flow properties, but also has a significant effect on the global properties, which are very different from the previous findings in 3-D and true 2-D systems (Daya & Ecke 2001; Song & Tong 2010; van der Poel *et al.* 2011, 2012, 2013; Chandra & Verma 2013).

The rest of this paper is organized as follows. The experimental set-up and measurement techniques are described in § 2. The main results are presented in § 3, which is divided into three parts. We first show the results obtained from the flow field and reversal measurements in § 3.1. The influences of geometric confinement on the local temperature fluctuation and the global heat transport will be presented in §§ 3.2 and 3.3. A summary of our findings comes in § 4.

2. Experimental apparatus and methods

The experiments were conducted in the range $8.6 \times 10^7 \leqslant Ra \leqslant 2.50 \times 10^9$ with the bulk temperature of the fluid (deionized and degassed water) T_c maintained at 40.0 °C,

corresponding to $Pr = 4.3$. The convection cells used in the experiments were similar to the one described in Xia, Sun & Zhou (2003). Briefly, they were of rectangular shape and were built independently with their own Plexiglas side walls and conducting plates (but of identical design), where the bottom plates were heated with constant power and the top plates were kept at constant temperature. The height H and length L of the cells were the same and fixed at 12.6 cm, thus the aspect ratio $\Gamma_\parallel$ $(=L/H)$ in the plane parallel to the large-scale circulation (LSC) plane is one; whereas the width W of the cells had values 7.56, 3.84, 2.56, 1.92 and 1.27 cm, giving rise to aspect ratios in the plane perpendicular to the LSC plane ($\Gamma_\perp = W/H$, hereafter simply Γ) of 0.6, 0.3, 0.2, 0.15 and 0.1, respectively. With these geometric configurations, the confinement on the flow is expected to increase as Γ decreases. Having exactly the same height is one important feature of the present study, as it allows measurements in different cells to be made over exactly the same range of Ra, so that results obtained from different cells can be compared directly.

To obtain an overall picture of the confinement effects on the flow dynamics, we made 2-D velocity measurements in the vertical plane midway between the front and back walls of the convection cell at two selected aspect ratios, i.e. $\Gamma = 0.3$ and 0.15, using a commercial particle image velocimetry (PIV) system that has been introduced elsewhere (Xia *et al.* 2003). In the PIV measurements, the fluid was seeded with polyamide particles of 50 μm in diameter. Each flow field contained 127 × 127 velocity vectors and a total of 10 000 vector maps were acquired with a sampling rate ∼2 Hz. The statistical behaviour of flow reversal, a phenomenon that the LSC suddenly reverses its flow direction in an erratic manner (Sreenivasan, Bershadskii & Niemela 2002; Brown & Ahlers 2007; Xi & Xia 2007), were studied with the so-called temperature contrast method (Sugiyama *et al.* 2010; Ni, Huang & Xia 2015). For ease of presentation, the details of this technique will be described in § 3.1. The temperature fluctuations in the cell centre were measured with a small thermistor with a size of 200 μm. Except in the PIV measurements, where a transparent window was required, several layers of thermal insulation were wrapped to the whole convection cell to prevent the heat leakage. To minimize influence from the surroundings, all the measurements were made in a thermostat with a stability of better than 0.1 °C.

3. Results and discussions

3.1. *Flow dynamics*

It is one's intuition that the flow dynamics should strongly depend on geometry. To find out how the flow dynamics responds to geometric confinement, we show in figure 1(*a–c*) the PIV-measured mean velocity fields for $\Gamma = 0.3$ (the unconfined case) and 0.15. The first thing we can see is that there exists a well-defined LSC with two counter-rotating corner rolls in the $\Gamma = 0.3$ cell, as found in previous studies with similar aspect ratios (Xia *et al.* 2003; Sugiyama *et al.* 2010). For the $\Gamma = 0.15$ cell, however, one finds a quite different flow pattern in the long time-averaged field: The single-roll structure has disappeared, instead, we have a four-roll structure. One way such a four-roll pattern in the mean field can arise is for the LSC to frequently reverse its flow direction, which had been experimentally demonstrated in an earlier study (Sun, Xia & Tong 2005*b*). Indeed, by taking short time averages of the instantaneous velocity fields, we can obtain LSCs with both clockwise and counter-clockwise flow directions in the $\Gamma = 0.15$ cell (see figure 1*c* for the counter-clockwise case), which was also illustrated in a recent numerical study with a similar Γ (Kaczorowski, Chong & Xia 2014). The second difference between these two Γ cells is that the

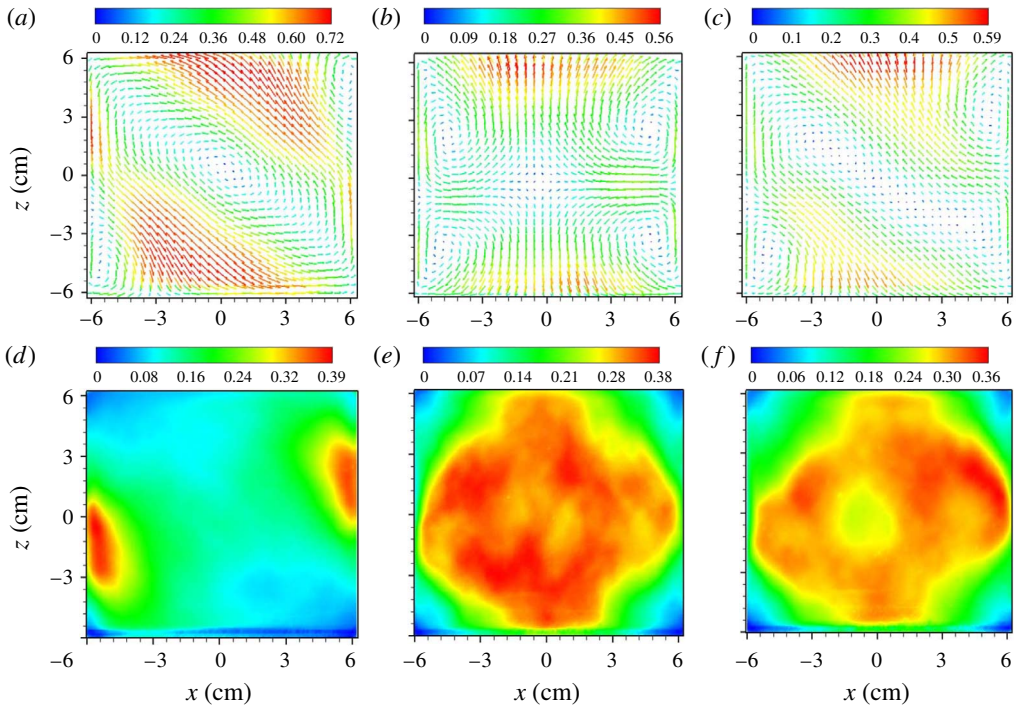

FIGURE 1. (Colour online) Coarse-grained vector maps of mean velocity field (*a–c*) and the corresponding contour maps of the r.m.s. velocity field (*d–f*) at $Ra = 1.1 \times 10^9$. (*a*,*d*) $\Gamma = 0.3$ cell by long time averaging; (*b*,*e*) $\Gamma = 0.15$ cell with a four-roll pattern by long time averaging; (*c*,*f*) $\Gamma = 0.15$ cell with a well-identified LSC by short time averaging. The velocity is coded in both colour scale and vector length in units of cm s^{-1}. The r.m.s. velocity is represented by the colour coding in units of cm s^{-1}.

magnitude of the time-averaged LSC is smaller for $\Gamma = 0.15$, as indicated clearly by the scale bar. While the increased drag force from the walls can certainly slow down the flow, a more fluctuating flow can also result in a smaller mean velocity. Larger fluctuations in the flow field for small Γ are evident in the root-mean-square (r.m.s.) velocity field (see figure 1*d–f*), which shows that the fluctuations in the bulk of the $\Gamma = 0.15$ cell become stronger and the region of strong fluctuations also becomes larger. It has been found in Xia *et al.* (2003) that larger velocity fluctuations are associated with plume clusters, therefore the r.m.s. velocity fields measured here indicate that there are more thermal plumes going through the bulk region in the highly confined geometry, rather than rising and falling along the side walls as is the case for larger Γ. Note that the reversal of the LSC could also contribute to a larger velocity fluctuation in the bulk region. However, we found that the r.m.s. velocity field in the $\Gamma = 0.15$ cell for the situation when a LSC can still be identified by short time averaging is quite similar to the one with a four-roll pattern (see figure 1*e*,*f*), suggesting that the major contributors for larger fluctuations in the bulk flow are the thermal plumes.

That flow reversals become more probable in quasi-2-D cells with smaller Γ was also observed in some previous studies (Vasilev & Frick 2011; Wagner & Shishkina 2013; Kaczorowski *et al.* 2014), but their statistical properties have not been examined.

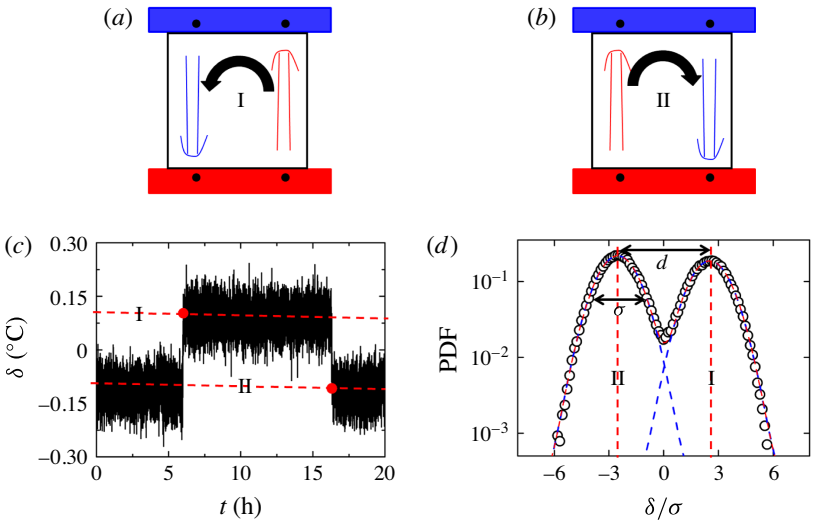

FIGURE 2. (Colour online) A schematic sketch of the reversal process changing from (*a*) state I to (*b*) state II. (*c*) A typical time series of the temperature contrast δ between the two sensors embedded in the bottom plate for $Ra = 1.1 \times 10^9$. The red solid circles indicate detections of flow reversal events based on the criteria described in the text. The red dashed lines indicate the two flow states I and II shown in (*a*) and (*b*), respectively. (*d*) The corresponding PDF of the data shown in (*c*). The blue dashed lines are two independent Gaussian function fits to the data and the red solid line is the superposition of them. It is seen that the data can be excellently fitted with a double-Gaussian function. See text for the explanations of d and σ. Note that similar results were obtained from the top plate.

Here, we used the temperature contrast method (Sugiyama *et al.* 2010; Ni *et al.* 2015) to detect flow reversal events over long time periods. This method is based on the idea that a region where cold plumes impinge should have a lower temperature than that where hot plumes emit. As illustrated in figure 2, when the LSC circulates in the counter-clockwise direction (state I as sketched in figure 2*a*), the temperature in the left side of the bottom plate is lower than that in the right side; when the flow reverses its circulation directing and changes to state II (figure 2*b*), the temperature in the left side becomes higher. Therefore, the temperature contrast $\delta = T_{right} - T_{left}$ will change its sign during a reversal event and thus is a good indicator of reversals (see figure 2*c*). Besides the sign change of δ, we set three more criteria to count true reversal events. The first one is that the two circulation states can be clearly distinguished from each other. This is quantified with the PDF of δ, as shown in figure 2(*d*). To be specific, the distance d between the two most probable values in the PDF should be larger than the r.m.s. value σ so that the two peaks can be clearly distinguished, where d and σ were obtained by a double-Gaussian function fit as shown in figure 2(*d*). The second criterion is that when the flow changes from one state to the other, δ should first crossover the peak, i.e. the value of δ should be larger (smaller) than the peak value in the PDF corresponding to state I (II). The third one is that the flow should stay at the new state for more than one turnover time t_{LSC} of the LSC, which was obtained from the correlation function of the temperature signals inside the plates (Brown, Funfschilling & Ahlers 2007). With these criteria, we are ready to examine the flow reversals quantitatively.

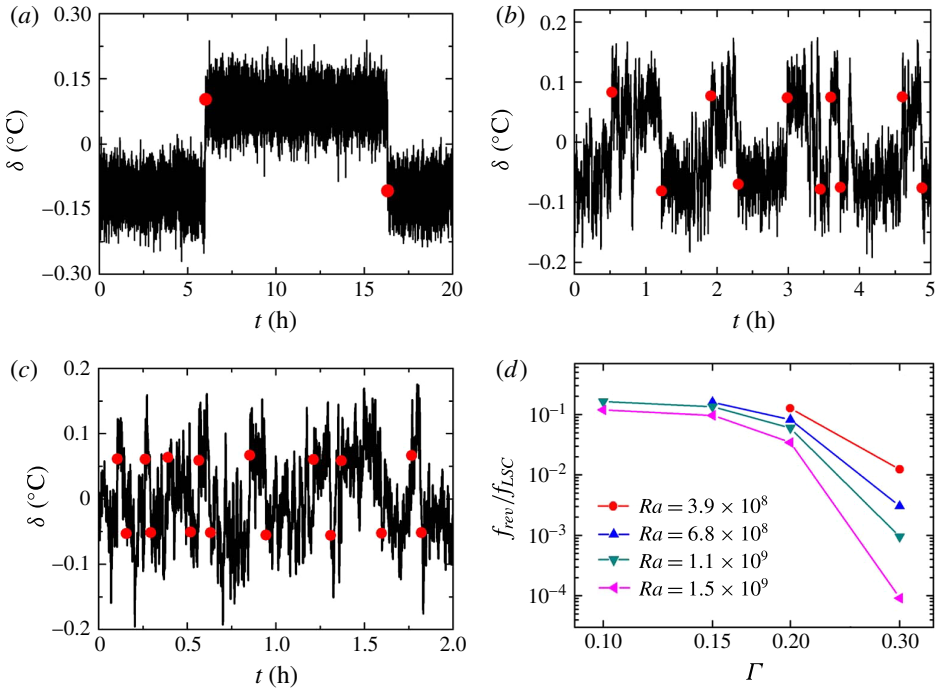

FIGURE 3. (Colour online) Examples of flow reversals at $Ra = 1.1 \times 10^9$ for (*a*) $\Gamma = 0.3$, (*b*) $\Gamma = 0.2$ and (*c*) $\Gamma = 0.15$. The red solid circles indicate detections of flow reversal events based on the criteria described in the text. (*d*) The normalized flow reversal frequency f_{rev}/f_{LSC} as a function of Γ for different Ra, where $f_{rev} = 1/\langle\tau\rangle$, $f_{LSC} = 1/t_{LSC}$, and $\langle\tau\rangle$ is the mean time interval between successive reversals.

We first show in figure 3(*a–c*) some examples of flow reversals at $Ra = 1.1 \times 10^9$ for $\Gamma = 0.3$, 0.2 and 0.15, respectively. It is seen clearly that the LSC reverses its circulating direction with a drastically increased frequency as Γ decreases, which is quantified in figure 3(*d*). However, when Γ is further reduced from 0.15 to 0.1, the reversal frequency does not show a significant increase anymore, so we do not show the examples for $\Gamma = 0.1$ here. It is further observed in figure 3(*d*) that the increase in the reversal frequency is Ra-dependent: the higher Ra becomes, the larger the increase (by more than 1000-fold for the highest value of Rayleigh number reached in the experiment), suggesting that the impact of confinement on the LSC dynamics is stronger for higher Ra. Note that the measurements in smaller Γ cells did not go to lower Ra, because σ becomes comparable with d in these cases, thus the first criterion is not satisfied anymore. This is a limitation of the measurement technique. We also remark that no flow reversal was observed in the $\Gamma = 0.6$ cell, even with a long time measurement of up to $15\,000 t_{LSC}$ (more than two weeks) at $Ra = 2.8 \times 10^8$, at which flow reversals are supposed to have a higher probability of occurrence than at higher Ra (Sugiyama *et al.* 2010; Ni *et al.* 2015).

In a recent study using quasi-2-D cells similar to the ones used in the present experiment, Ni *et al.* (2015) have shown that the mean time interval between successive reversals $\langle\tau\rangle$ follows a stochastic process, i.e. $\langle\tau\rangle/t_{LSC} = C_p(\Gamma)\exp[(d/2\sigma)^2]$, where d is taken as the relative strength of the LSC and σ is its fluctuation. Figure 4 shows the data $\langle\tau\rangle/t_{LSC}$ versus $(d/2\sigma)^2$ for different Γ cells in a semi-log plot.

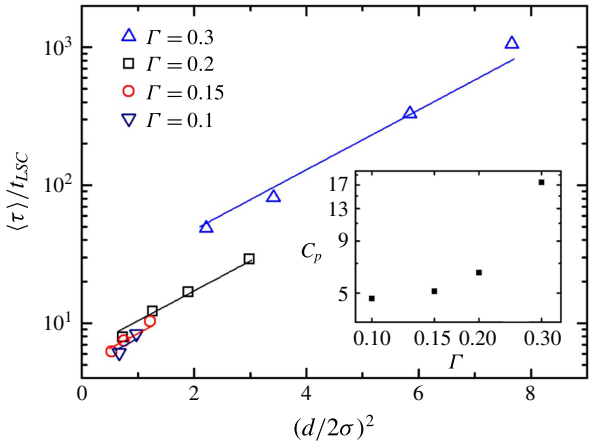

FIGURE 4. (Colour online) A semi-log plot of the normalized mean time interval between successive reversals $\langle\tau\rangle/t_{LSC}$ as a function of $(d/2\sigma)^2$ for different Γ. The solid lines are fittings to individual data sets according to the formula $\langle\tau\rangle/t_{LSC} = C_p(\Gamma)\exp[(d/2\sigma)^2]$ obtained in a model developed by Ni *et al.* (2015) recently. Inset: The fitting coefficient C_p versus Γ.

It is seen that the data can be nicely fitted with the formula above, with a strong Γ-dependent prefactor C_p, as shown in the inset, indicting that the model developed in Ni *et al.* (2015) can also well describe the reversal behaviours in a highly confined geometry. Since the value of d/σ can be used to characterize the stability of the LSC, we further examine their values separately to see how confinement affects the properties of the LSC. It is seen in figure 5 that as Γ decreases, d decreases on one hand, and σ increases on the other, which suggests that LSC becomes weaker and experiences stronger fluctuations in highly confined geometry, thus confirming the PIV-measured results. As d is essentially the temperature difference between the left and right sides of the conducting plates, smaller d also suggests that the temperature is more uniform in the plate for small Γ cells, consistent with the findings in Huang *et al.* (2013).

In figure 6, we show the PDFs of time interval between successive reversals τ/t_{LSC} for $\Gamma = 0.2$ and 0.15 cells on a semi-log scale. It is seen that the data for both Γ are in good agreement with the exponential function $p(\tau/t_{LSC}) \sim \exp(-\tau/t_{LSC})$. (The levelling off of the PDFs at the large values of τ/t_{LSC} is caused by the insufficient statistics.) These results indicate that flow reversals in the quasi-2-D geometry obey Poisson statistics as in the 3-D case (Sreenivasan *et al.* 2002; Brown & Ahlers 2007; Xi & Xia 2007), which suggests that it may be possible to develop a geometry-independent model to explain the apparently different LSC dynamics in different geometries.

3.2. *Local temperature fluctuations*

In Huang *et al.* (2013), it was simply mentioned that with decreasing Γ the local temperature fluctuation in the cell centre increases significantly and its PDF changes from exponential to Gaussian. Here, we present the details. Figure 7(*a*,*b*) shows the time series of temperatures measured at the cell centre for $Ra = 1.1 \times 10^9$ and $Ra = 8.6 \times 10^7$, respectively. It is seen clearly that the fluctuations in small

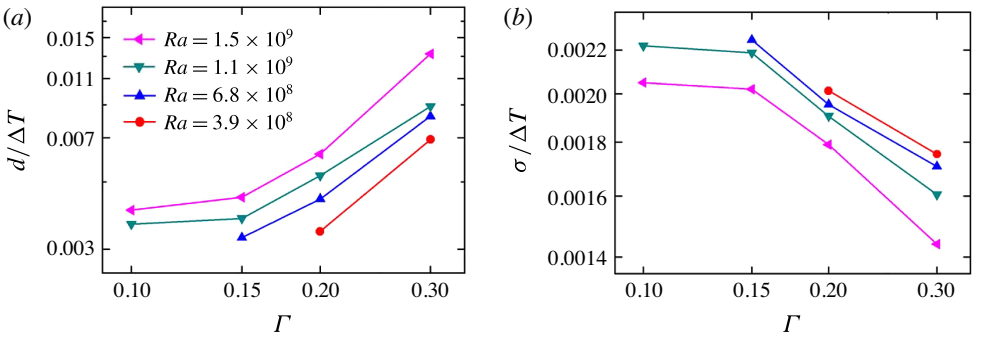

FIGURE 5. (Colour online) (*a*) The strength of the LSC d and (*b*) its fluctuation σ normalized by the global temperature difference ΔT as a function of Γ for different Ra. Note that ΔT for different Γ cells are the same for the same Ra, as they have the same height.

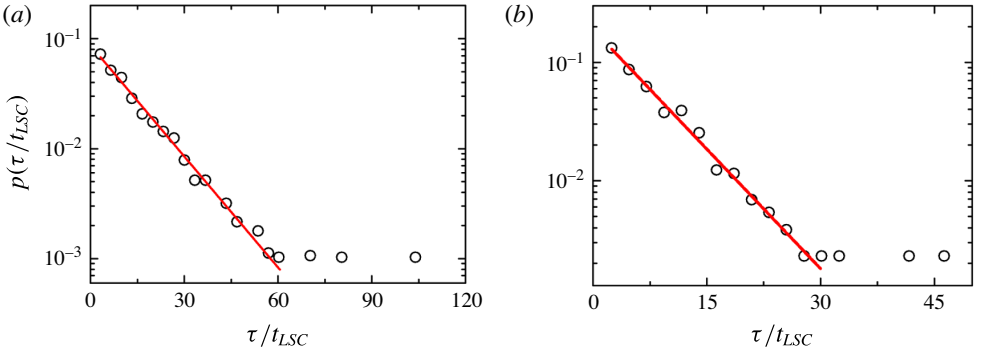

FIGURE 6. (Colour online) PDFs of the normalized time interval between successive flow reversals at $Ra = 1.1 \times 10^9$ for (*a*) $\Gamma = 0.2$ and (*b*) $\Gamma = 0.15$, respectively. The straight lines indicate exponential fittings.

Γ cells are stronger than those in large ones. Besides the change in fluctuation magnitude, the corresponding PDFs (shown in figure 7*c*,*d*) also change their forms: as Γ is reduced, there is a transition from (stretched) exponential to Gaussian-like. The strong geometric dependency of the temperature fluctuation PDF found in the quasi-2-D system is consistent with a recent numerical simulation using similar geometries (Kaczorowski *et al.* 2014), but quite different from previous studies conducted in 3-D systems, in which a universal form for different geometries was observed (Daya & Ecke 2001; Song & Tong 2010). The functional form of the temperature fluctuation PDF is one important hallmark for different flow states (Heslot, Castaing & Libchaber 1987; Castaing *et al.* 1989; Massaioli, Benzi & Succi 1993) and the plume distribution in the convection cell (Xia & Lui 1997), thus these changes confirm that the flow state has been changed and/or there are more plumes passing though the cell centre as a result of confinement.

To examine these changes quantitatively, we plot the Ra-dependence of the normalized r.m.s. temperature $\sigma_c/\Delta T$ and their flatness values in figure 8. From figure 8(*a*), one can see that while the magnitude of $\sigma_c/\Delta T$ increases as Γ decreases, its Ra-scaling exponent in general decreases (see table 1 for detailed values).

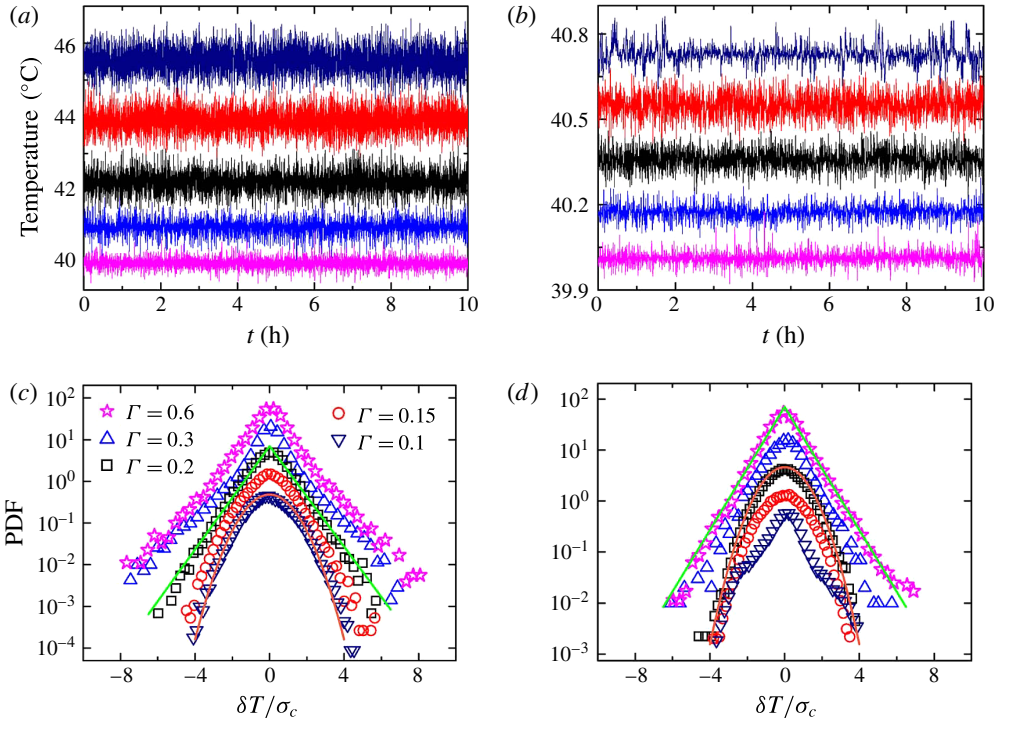

FIGURE 7. (Colour online) (*a*,*b*) Time series of temperatures measured at the cell centre for (*a*) $Ra = 1.1 \times 10^9$ and (*b*) $Ra = 8.6 \times 10^7$. From top to bottom, $\Gamma = 0.1$, 0.15, 0.2, 0.3 and 0.6. (*c*,*d*) The corresponding PDFs of temperature fluctuations shown in (*a*,*b*): (*c*) $Ra = 1.1 \times 10^9$ and (*d*) $Ra = 8.6 \times 10^7$. Note that the data for different Γ have been upshifted for clarity. The green and orange lines represent exponential and Gaussian fits, respectively.

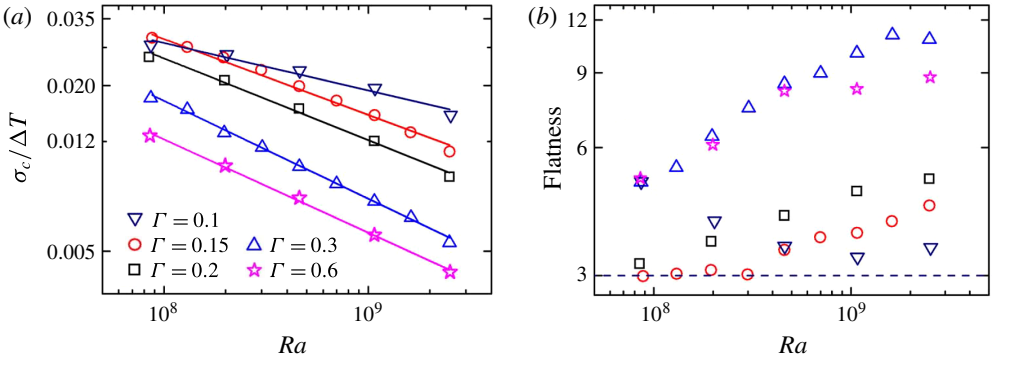

FIGURE 8. (Colour online) (*a*) Normalized temperature fluctuation $\sigma_c/\Delta T$ at the cell centre as a function of Ra for different Γ. The solid lines represent power-law fits to the individual data sets. (*b*) The corresponding flatness versus Ra.

Large variations in the Ra dependency of temperature fluctuations due to geometric effects have also been found in earlier studies (Daya & Ecke 2001; Song & Tong 2010). We note that the scalings for the $\Gamma = 0.6$ and 0.3 cells are the same as

Γ	A	$\alpha \pm 0.002$	$C_1 \pm 0.005$	$C_2 \pm 0.02$	B	$\beta \pm 0.01$
0.6	0.173	0.286	0.029	0.20	6.56	−0.35
0.3	0.152	0.291	0.033	0.17	12.43	−0.35
0.2	0.216	0.277	0.022	0.25	6.04	−0.30
0.15	0.264	0.269	0.017	0.29	4.75	−0.27
0.1	0.267	0.270	0.018	0.31	0.69	−0.17

TABLE 1. Fitting coefficients for the single power law $Nu = ARa^{\alpha}$, the combined power law $Nu = C_1 Ra^{1/3} + C_2 Ra^{1/4}$ and the normalized temperature fluctuation $\sigma_c/\Delta T = BRa^{\beta}$ measured in different Γ cells. For an easier data referring, the uncertainties presented here are the maximum values of the fitting errors among all the cells.

those found in a recent simulation of turbulent RB convection in a cubic geometry (Kaczorowski *et al.* 2014), but very different from the value −0.49 reported in Daya & Ecke (2001) in a convection cell with square cross-section. The $\Gamma = 0.3$ cell also has similar flatness values with the $\Gamma = 0.6$ cell (see figure 8*b*), suggesting that the convective flow has not sensed the confinement effects from the walls for $\Gamma = 0.3$. However, when Γ is further reduced, there is a sudden drop in the flatness values; and these values gradually decrease to ∼3 (Gaussian case) for smaller Γ and lower Ra, which is consistent with the change in the form of temperature fluctuation PDF shown in figure 7. Special attention is paid to the abnormal Ra dependence of flatness in the $\Gamma = 0.1$ cell, which is also reflected in its very different time series signals and the bimodal shaped PDF at $Ra = 8.6 \times 10^7$. Based on the recent finding by Chong *et al.* (2015), these strange behaviours for $\Gamma = 0.1$ could be due to the fact that the LSC no longer exists in this case.

3.3. *Heat transport*

We now examine the influences of spatial confinement on the heat transport properties. Figure 9 shows a semi-log plot of the compensated Nu versus Ra for different Γ cells. As the heat transfer in a cubic cell (i.e. $\Gamma = 1$) is identical to that in a cylinder (Qiu & Xia 1998*b*), for clarity and easy comparison, we plot in figure 9 the results measured in a cylindrical cell of $\Gamma = 1$ (Wei, Ni & Xia 2012), which is the most commonly used geometry in the study of turbulent RB convection. From figure 9, we find that: (i) the data for the $\Gamma = 0.6$ cell collapse well with those measured in the $\Gamma = 1$ cell; (ii) Nu first decreases a little when Γ is changed from 0.6 to 0.3 and then increases significantly afterwards, up to 17 % for the parameter range explored in the present study. Note that the Nu data have been reported in Huang *et al.* (2013). We plot them here in a different form to understand the confinement effects in turbulent thermal convection from a different point of view.

The solid lines in figure 9 represent power-law fits $Nu = ARa^{\alpha}$ to the measured data with the scaling exponent α varying from 0.27 to 0.29 (see table 1 for detailed values). These values are in general agreement with those found in previous studies in the same parameter ranges of Ra and Pr (Ahlers, Grossmann & Lohse 2009). We recall that the Grossmann–Lohse (GL) model splits the globally averaged dissipation rate into bulk and boundary layer (BL) contributions and suggests that different linear combinations of power laws for different parameter ranges should be used for the Nu–Ra fitting (Grossmann & Lohse 2000). Based on this idea, we fit to each set of data with a combination of two power laws proposed in the GL model, i.e.

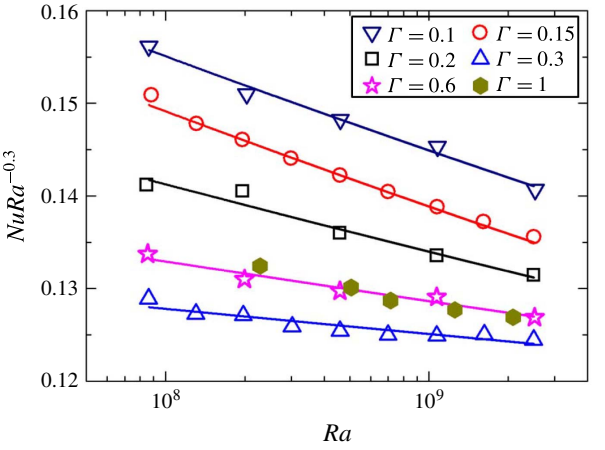

FIGURE 9. (Colour online) Compensated Nu as a function of Ra from different Γ cells as indicated by different symbols. The solid lines are power-law fits to individual data sets. The solid hexagons are the results measured in a cylindrical cell of $\Gamma = 1$ (Wei, Ni & Xia 2012).

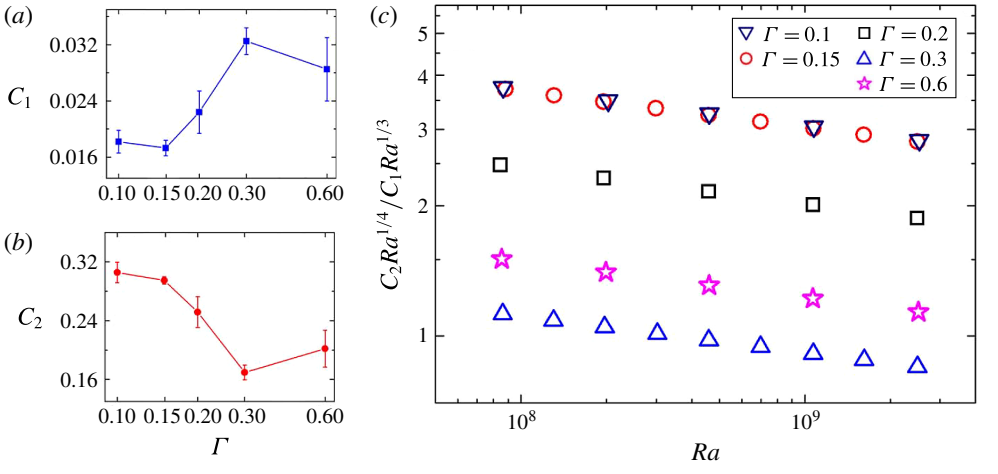

FIGURE 10. (Colour online) Fitting coefficients for the combined power law $Nu = C_1Ra^{1/3} + C_2Ra^{1/4}$ as a function of Γ: (*a*) C_1 and (*b*) C_2. (*c*) The ratio between $C_2Ra^{1/4}$ and $C_1Ra^{1/3}$ versus Ra in different Γ cells.

$Nu = C_1Ra^{1/3} + C_2Ra^{1/4}$, in which $C_1Ra^{1/3}$ and $C_2Ra^{1/4}$ represent the contributions from the bulk and BLs, respectively. The obtained fitting coefficients C_1 and C_2 for different Γ are plotted in figures 10(*a*) and 10(*b*), respectively (see table 1 for detailed values). It is seen that the Γ dependencies of C_1 and C_2 have an opposite trend: the decrease (increase) in C_1 is accompanied by an increase (decrease) in C_2. Interestingly, the behaviour of C_2 is similar to that of the global Nu: It first decreases when Γ is changed from 0.6 to 0.3 and then increases with decreasing Γ afterwards (see figure 1 in Huang *et al.* (2013)). This is because in the present parameter range, the heat transport, in terms of the energy dissipation rate, is dominated by

the contributions from the boundary layers, which is supported by comparing the magnitudes between $C_1Ra^{1/3}$ and $C_2Ra^{1/4}$ as shown in figure 10(*c*). The change in the ratio of $C_2Ra^{1/4}$ over $C_1Ra^{1/3}$ as Γ is decreased suggests that the confinement increases the contribution from the BLs in the global heat transport and weakens that from the bulk. This result is consistent with the finding in Huang *et al.* (2013), in which it was found that the confinement suppresses the large-scale turbulent flow in the bulk and enables thermal plumes (commonly viewed as detached thermal BLs) to pass through the entire cell, rather than being confined in its periphery.

Why have such significant changes in *Nu* not been observed in previous studies in 3-D and true 2-D systems? Note that even for the smallest Γ explored in the present study, the width of the cell (its smallest dimension) is still much larger than the thermal boundary layer thickness, therefore it is unlikely that the geometric effects will directly lead to any change in the BLs and hence *Nu*. Thus, the reasons must be connected to the flow structures. It has been shown by Huang *et al.* (2013) that the confinement restricts the plume's movement near the BLs into a 1-D motion, resulting in the formation of highly coherent plumes. These highly coherent plumes turn out to have a stronger interaction with the BLs, which is supported by the mean velocity fields as shown in figure 1. It is seen that in the $\Gamma = 0.3$ cell the mean flow near the boundary layers has a large horizontal component, whereas in the $\Gamma = 0.15$ case, the mean flow is largely perpendicular and thus perturbs the BLs directly. Therefore, geometric confinement in the quasi-2-D geometry not only changes the morphology and dynamics of thermal plumes, but also strengthens the interaction between the flow structures in the bulk and the BLs, both of which have not been observed in previous studies in 3-D systems. This explains why these studies found a weak Γ effect on heat transport. In the true 2-D case, there is no lateral confinement of the plumes when the aspect ratio is changed. As the coherent properties of plumes are not modified in this case but the flow structures are changed as a result of the aspect ratio variation, *Nu* is found to be sensitive to the nature of the flow structures in the 2-D geometry (van der Poel *et al.* 2011, 2012).

In a recent numerical simulation of 2-D turbulent convection (Chandra & Verma 2013), extremely large fluctuations and even negative values of global *Nu* were observed during the flow reversal processes, which was attributed to the strong geometric constraints to the flow. Since the confinement also leads to more frequent flow reversals, it would be interesting to examine the instantaneous *Nu* for different Γ during reversals. As we can see in figure 11(*a*,*b*), neither negative values nor very large fluctuations are observed in the time series of instantaneous *Nu* for all the cases, which is also reflected by their PDFs, shown in figure 11(*c*,*d*). Although there is a trend that the fluctuations of instantaneous *Nu* increase as Γ decreases, the fluctuation values for all the Γ and the differences between them are so small that they are all within 1 % of the mean values. These results further suggest that the quasi-2-D geometry is different from the true 2-D case.

4. Conclusion

In summary, our experiments reveal rich physics in quasi-2-D turbulent RB flow under geometric confinement.

(i) With the increasing degree of confinement, the large-scale flow slows down and there are more plumes traveling through the bulk region. Moreover, the LSC reverses its circulation direction more frequently in smaller Γ cells, by more than 1000-fold for the highest value of Rayleigh number reached in the experiment.

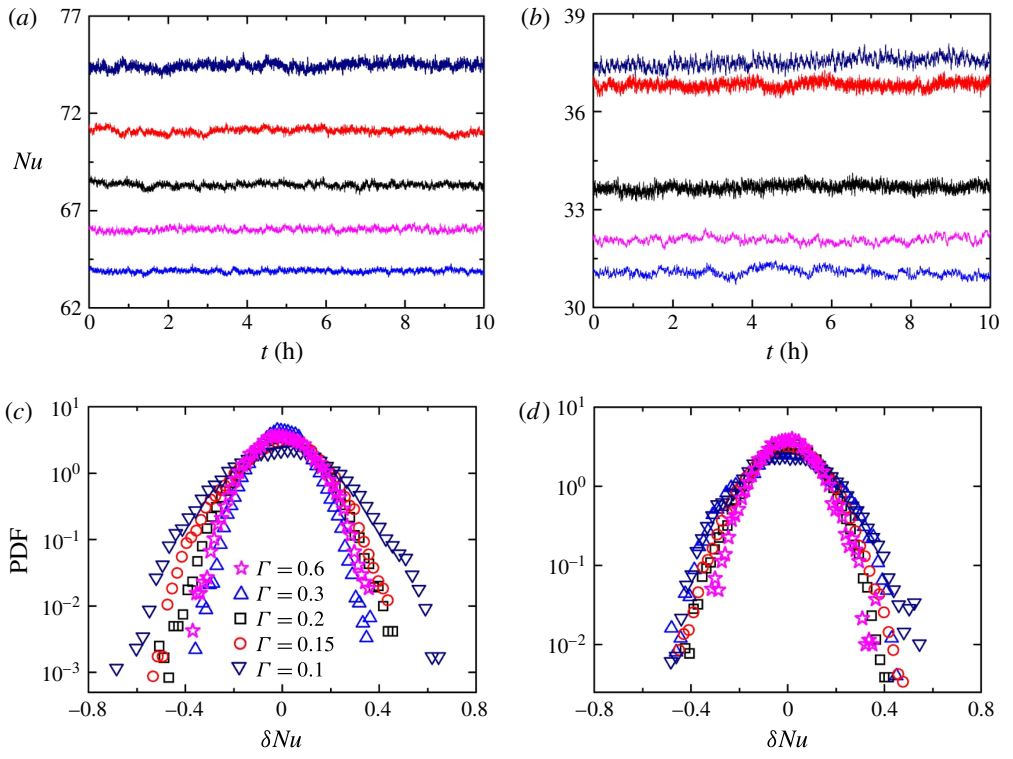

FIGURE 11. (Colour online) (*a*,*b*) Time series of instantaneous Nu for (*a*) $Ra = 1.1 \times 10^9$ and (*b*) $Ra = 8.6 \times 10^7$. From top to bottom, $\Gamma = 0.1$, 0.15, 0.2, 0.6 and 0.3. (*c*,*d*) The corresponding PDFs of the Nu fluctuations shown in (*a*,*b*): (*c*) $Ra = 1.1 \times 10^9$ and (*d*) $Ra = 8.6 \times 10^7$.

Despite the significant changes in the flow pattern and dynamics, it is found that the reversal process still follows Poissonian statistics, as in the 3-D system, and the reversal frequency could be well described by the stochastic model of Ni *et al.* (2015), which is closely related to the models used in other geometries (Brown & Ahlers 2007; Song *et al.* 2014). These common features are good circumstantial evidence for a potentially general model of LSC dynamics in different geometries.

(ii) The impact of geometric confinement on the flow dynamics is also reflected in the local temperature fluctuation. It is found that the bulk temperature fluctuations in different Γ cells differ from each other not only in the magnitude and Ra-dependent scaling, but also in the PDF shapes. These changes are the outcome of the changes in the flow state and/or plume distribution in the convection cell.

(iii) Despite a slower flow, remarkable enhancement of heat transport is observed. By analysing the Nu–Ra behaviours according to the GL model, our results suggest that as Γ decreases, the relative weight of the boundary layer contribution to the global heat transport increases and at the same time that from the bulk decreases. In addition, we did not observe large variations nor negative values in global Nu during the reversal processes as found in true 2-D systems, which provides another evidence for the difference between the quasi-2-D and the true 2-D geometries.

These geometric confinement induced changes in quasi-2-D turbulent RB convection show that the interaction between the LSC, the thermal plumes and the BLs in thermal convection is more complicated than previous thought. These striking phenomena have not been observed in previous studies in 3-D and true 2-D systems, and could not be accounted for with the existing models for aspect ratio dependence (Grossmann & Lohse 2003; Ching & Tam 2006). We end by stressing that our present understanding of the confinement effects in quasi-2-D turbulent convection are 2-fold: the first is the changes in the morphology and dynamics of thermal plumes and the modification of the flow structures in the bulk; the second is the strengthening of the interaction between the flow structures in the bulk and the BLs. Given this, the influence of geometric confinement in the small-Γ limit would be an interesting topic for future studies.

Acknowledgements

We thank S.-Q. Zhou and X.-D. Shang for kindly making their PIV apparatus available to us. We also thank F. Wang and L. Qu for their help with the experiments. This work was supported by the Hong Kong Research Grants Council under grant nos CUHK 403712 and 404513.

REFERENCES

AHLERS, G., GROSSMANN, S. & LOHSE, D. 2009 Heat transfer and large-scale dynamics in turbulent Rayleigh–Bénard convection. *Rev. Mod. Phys.* **81**, 503–537.

BAILON-CUBA, J., EMRAN, M. S. & SCHUMACHER, J. 2010 Aspect ratio dependence of heat transfer and large-scale flow in turbulent convection. *J. Fluid Mech.* **655**, 152–173.

BROWN, E. & AHLERS, G. 2007 Large-scale circulation model for turbulent Rayleigh–Bénard convection. *Phys. Rev. Lett.* **98**, 134501.

BROWN, E., FUNFSCHILLING, D. & AHLERS, G. 2007 Anomalous Reynolds-number scaling in turbulent Rayleigh–Bénard convection. *J. Stat. Mech.* **2007**, P10005.

CASTAING, B., GUNARATNE, G., KADANOFF, L. P., LIBCHABER, A. & HESLOT, F. 1989 Scaling of hard thermal turbulence in Rayleigh–Bénard convection. *J. Fluid Mech.* **204**, 1–30.

CHANDRA, M. & VERMA, M. K. 2013 Flow reversals in turbulent convection via vortex reconnections. *Phys. Rev. Lett.* **110**, 114503.

CHILLÀ, F. & SCHUMACHER, J. 2012 New perspectives in turbulent Rayleigh–Bénard convection. *Eur. Phys. J.* E **35**, 58.

CHING, E. S. C. & TAM, W. S. 2006 Aspect-ratio dependence of heat transport by turbulent Rayleigh–Bénard convection. *J. Turbul.* **7**, N72.

CHONG, K.-L., HUANG, S.-D., KACZOROWSKI, M. & XIA, K.-Q. 2015 Condensation of coherent structures in turbulent flows. *Phys. Rev. Lett.* **115**, 264503.

DAYA, Z. A. & ECKE, R. E. 2001 Does turbulent convection feel the shape of the container? *Phys. Rev. Lett.* **87**, 184501.

FUNFSCHILLING, D., BROWN, E., NIKOLAENKO, A. & AHLERS, G. 2005 Heat transport by turbulent Rayleigh–Bénard convection in cylindrical samples with aspect ratio one and larger. *J. Fluid Mech.* **536**, 145–154.

GROSSMANN, S. & LOHSE, D. 2000 Scaling in thermal convection: a unifying theory. *J. Fluid Mech.* **407**, 27–56.

GROSSMANN, S. & LOHSE, D. 2003 On geometry effects in Rayleigh–Bénard convection. *J. Fluid Mech.* **486**, 105–114.

HESLOT, F., CASTAING, B. & LIBCHABER, A. 1987 Transitions to turbulence in helium gas. *Phys. Rev.* A **36**, 5870–5873.

HUANG, S.-D., KACZOROWSKI, M., NI, R. & XIA, K.-Q. 2013 Confinement-induced heat-transport enhancement in turbulent thermal convection. *Phys. Rev. Lett.* **111**, 104501.

HUANG, Y.-X. & ZHOU, Q. 2013 Counter-gradient heat transport in two-dimensional turbulent Rayleigh–Bénard convection. *J. Fluid Mech.* **737**, R3.

KACZOROWSKI, M., CHONG, K.-L. & XIA, K.-Q. 2014 Turbulent flow in the bulk of Rayleigh–Bénard convection: aspect-ratio dependence of the small-scale properties. *J. Fluid Mech.* **747**, 73–102.

LOHSE, D. & XIA, K.-Q. 2010 Small-scale properties of turbulent Rayleigh–Bénard convection. *Annu. Rev. Fluid Mech.* **42**, 335–364.

MASSAIOLI, F., BENZI, R. & SUCCI, S. 1993 Exponential tails in two-dimensional Rayleigh–Bénard convection. *Europhys. Lett.* **21**, 305–310.

NI, R., HUANG, S.-D. & XIA, K.-Q. 2015 Reversals of the large-scale circulation in quasi-2D Rayleigh–Bénard convection. *J. Fluid Mech.* **778**, R5.

NIEMELA, J. J. & SREENIVASAN, K. R. 2006 Turbulent convection at high Rayleigh numbers and aspect ratio 4. *J. Fluid Mech.* **557**, 411–422.

NIKOLAENKO, A., BROWN, E., FUNFSCHILLING, D. & AHLERS, G. 2005 Heat transport by turbulent Rayleigh–Bénard convection in cylindrical cells with aspect ratio one and less. *J. Fluid Mech.* **523**, 251–260.

PODVIN, B. & SERGENT, A. 2015 A large-scale investigation of wind reversal in a square Rayleigh–Bénard cell. *J. Fluid Mech.* **766**, 172–201.

VAN DER POEL, E. P., STEVENS, R. J. A. M. & LOHSE, D. 2011 Connecting flow structures and heat flux in turbulent Rayleigh–Bénard convection. *Phys. Rev.* E **84**, 045303.

VAN DER POEL, E. P., STEVENS, R. J. A. M. & LOHSE, D. 2013 Comparison between two-and three-dimensional Rayleigh–Bénard convection. *J. Fluid Mech.* **736**, 177–194.

VAN DER POEL, E. P., STEVENS, R. J. A. M., SUGIYAMA, K. & LOHSE, D. 2012 Flow states in two-dimensional Rayleigh–Bénard convection as a function of aspect-ratio and Rayleigh number. *Phys. Fluids* **24**, 085104.

DU PUITS, R., RESAGK, C. & THESS, A. 2007 Breakdown of wind in turbulent thermal convection. *Phys. Rev.* E **75**, 016302.

QIU, X.-L. & XIA, K.-Q. 1998*b* Viscous boundary layers at the sidewall of a convection cell. *Phys. Rev.* E **58**, 486–491.

ROCHE, P., GAUTHIER, F., KAISER, R. & SALORT, J. 2010 On the triggering of the ultimate regime of convection. *New J. Phys.* **12**, 085014.

SONG, H. & TONG, P. 2010 Scaling laws in turbulent Rayleigh–Bénard convection under different geometry. *Europhys. Lett.* **90**, 44001.

SONG, H., BROWN, E., HAWKINS, R. & TONG, P. 2014 Dynamics of large-scale circulation of turbulent thermal convection in a horizontal cylinder. *J. Fluid Mech.* **740**, 136–167.

SREENIVASAN, K. R., BERSHADSKII, A. & NIEMELA, J. J. 2002 Mean wind and its reversal in thermal convection. *Phys. Rev.* E **65**, 056306.

SUGIYAMA, K., NI, R., STEVENS, R. J. A. M., CHAN, T. S., ZHOU, S.-Q., XI, H.-D., SUN, C., GROSSMANN, S., XIA, K.-Q. & LOHSE, D. 2010 Flow reversals in thermally driven turbulence. *Phys. Rev. Lett.* **105**, 034503.

SUN, C., REN, L.-Y., SONG, H. & XIA, K.-Q. 2005*a* Heat transport by turbulent Rayleigh–Bénard convection in 1 m diameter cylindrical cells of widely varying aspect ratio. *J. Fluid Mech.* **542**, 165–174.

SUN, C., XIA, K.-Q. & TONG, P. 2005*b* Three-dimensional flow structures and dynamics of turbulent thermal convection in a cylindrical cell. *Phys. Rev.* E **72**, 026302.

VASILEV, A. YU. & FRICK, P. G. 2011 Reversals of large-scale circulation in turbulent convection in rectangular cavities. *J. Expl Theor. Phys. Lett.* **93**, 330–334.

WAGNER, S. & SHISHKINA, O. 2013 Aspect-ratio dependency of Rayleigh–Bénard convection in box-shaped containers. *Phys. Fluids* **25**, 085110.

WEI, P., NI, R. & XIA, K.-Q. 2012 Enhanced and reduced heat transport in turbulent thermal convection with polymer additives. *Phys. Rev.* E **86**, 016325.

WU, X.-Z. & LIBCHABER, A. 1992 Scaling relations in thermal turbulence: the aspect-ratio dependence. *Phys. Rev.* A **45**, 842–845.

XI, H.-D. & XIA, K.-Q. 2007 Cessations and reversals of the large-scale circulation in turbulent thermal convection. *Phys. Rev.* E **75**, 066307.

XIA, K.-Q. 2013 Current trends and future directions in turbulent thermal convection. *Theor. Appl. Mech. Lett.* **3**, 052001.

XIA, K.-Q. & LUI, S.-L. 1997 Turbulent thermal convection with an obstructed sidewall. *Phys. Rev. Lett.* **79**, 5006–5009.

XIA, K.-Q., SUN, C. & CHEUNG, Y.-H. 2008 Large scale velocity structures in turbulent thermal convection with widely varying aspect ratio. In *Proceedings of the 14th International Symposium on Applications of Laser Techniques to Fluid Mechanics*.

XIA, K.-Q., SUN, C. & ZHOU, S.-Q. 2003 Particle image velocimetry measurement of the velocity field in turbulent thermal convection. *Phys. Rev.* E **68**, 066303.

ZHOU, Q., LIU, B.-F., LI, C.-M. & ZHONG, B.-C. 2012 Aspect ratio dependence of heat transport by turbulent Rayleigh–Bénard convection in rectangular cells. *J. Fluid Mech.* **710**, 260–276.